Transactions of the Indian National Academy of Engineering
https://doi.org/10.1007/s41403-024-00493-4

ORIGINAL ARTICLE

Effect of Efficiency of a Thermophotovoltaic GaSb Solar Cell Subjected to 1D Photonic Crystal Filter and Double/Multi-Layer Anti-Reflective Coatings

Fabrice Kwefeu Mbakop[1,2] · Gustave Assoualaye[2] · Ahmat Tom[3] · Aristide Tolok Nelem[4] · Jean Benjamin Bidias[2] · Liviu Leontie[5] · Felicia Iacomi[5] · Noel Djongyang[2]

Received: 10 February 2024 / Accepted: 29 June 2024

Abstract

Increasing the efficiency and electrical power density of thermophotovoltaic devices relies on recent advances in photovoltaic cell materials and technology. The study of the effect of optical properties and the impact on the performance of GaSb cell is presented in this work. However, in this type of system, the infrared radiation transformed into electricity corresponds to the GaSb cell spectrum. It can be done in several ways. The first means is that of an optical filter (Si/SiO_2). This structure is composed of ten periods. The second means are the double and multiple anti-reflection coatings. The temperature measured on the surface of the emitter was 1500 K in the operating condition for which wavelength is ranging from 800 to 1800 nm. The matrix transfer method enables the analysis of the optical properties behavior of each system in order to study the incidence variation. However, the highest incidence angle of for the anti-reflective coatings was limited to 30º. In addition, the electrical performances of the GaSb cell have been studied and compared. The current density for a cell without anti-reflective coating was 27.6 mA/cm^2, while for DLARC and MLARC coatings were 38.6 mA/cm^2 and 39.6 mA/cm^2 respectively. However, the optical filter itself generates a short-circuit current density of 42.6 mA/cm^2, significantly higher than the other three, which gives it an efficiency of 24.56%.

Keywords Antireflection coatings · GaSb cell · Spectral filter · Photonic crystal · Transfer matrix method · Thermophotovoltaic

Introduction

The conversion of electromagnetic waves into electricity from photovoltaic (PV) systems is crucial to meet the world's energy needs (Donne et al. 2013). However, PV solar cell exhibits a number of drawbacks, including a high initial cost, a large installation area, and the low conversion efficiency. Today the PV systems market is dominated by crystalline silicon PV cells, which represent about 80–85% in the world (Donne et al. 2013; Sathya and Swarna Priya 2019). The silicon PV cells are able to absorb 90% of incident light with wavelengths between 400 to 1200 nm.

However, only 12 to 18% of the radiation emitted by the sun is transmitted to the silicon cell. This radiation is subsequently transformed into electricity. The remaining radiations are converted into thermal energy, raising the temperature of the PV and causing a short circuit current density (J_{SC}) that rises by 0.06 to 0.1% degrees Celsius, while lowering the amount of electrical energy produced

✉ Fabrice Kwefeu Mbakop
mbakop.fabrice@yahoo.fr

1 Department of Renewable Energy, Higher Institute of Agriculture, Forestry, Water and Environment University of Ebolowa, Ebolowa, Cameroon

2 Department of Renewable Energy, National Advanced School Of Engineering, University of Maroua, Maroua, Cameroon

3 Department of Energy Engineering, University Institute of Technology (UIT), University of Ngaoundere, PO Box 455, Ngaoundere, Cameroon

4 Department of Renewable Energy, Higher Technical Teachers, Training College (HTTTC) of Ebolowa, University of Ebolowa, P.O. Box 886, Ebolowa, Cameroon

5 Faculty of Physics, Alexandru Ioan Cuza University of Iasi, 11 Carol I Blvd., 700506 Iasi, Romania

Published online: 27 July 2024

(Sathya and Swarna Priya 2019). In 1970, Wolf (1976) proposed a fusion technique between photovoltaic and thermal systems to overcome the problem. This method is known as a thermophotovoltaic energy system. This method is broadly known as photovoltaic energy generation. Other kind innovation was Thermovoltaics. Thermophotovoltaic (TPV) technology has received widespread attention due to their use in direct conversion of thermal energy radiated from a high-temperature source into electricity using PV cells (Donne et al. 2013; Belhadj et al. 2022; Coutts 2001; Pirvaram et al. 2021). TPV device is made up PV cells, a selective filter, and heat source that is thought to be a perfect blackbody. In a TPV device, the heat is close to the PV sensor as in photovoltaic solar systems, this phenomenon allows for a high value of photon flux which results in a high radiated power density. Semiconductors with low bandgap energy (Eg) are generally used in the design of PV cells, because the surface temperature of these cells varies between 1000 and 2000 K. These semiconductors include GaSb, InGaAs, and InGaAsSb (Zenker et al. 2001). Therefore, efficiency and electrical power of TPV devices can be optimized by adding between the transmitter and the diode a spectral filter or anti-reflective coatings (ARC), which transmit only the convertible spectrum. For design of optical filters, 1D, 2D or 3D photonic crystals are very often used (Belhadj et al. 2022).

In literature, there are several works involving filters, we have among others PhC Si/SiO_2 (Babiker et al. 2014; Tchoffo et al. 2022), PhC TiO_2/SiO_2 (Mbakop et al. 2016, 2017), which only involves dielectric-dielectric materials. We also find Ag/SiO2 metal-dielectric filters (Zhang et al. 2020; Gupta et al. 2021). Some work has focused on comparative studies of the performance of optical filters, Mbakop et al. (2020) present a comparative study between Si/SiO_2 and TiO_2/SiO_2 optical filters applied in TPV devices.

In addition to the spectral filters used in TPV systems, anti-reflective coatings applied to PV cells also help increase cell output performance.

Therefore, to improve the optical properties (reflection, transmission), a dielectric material having a thin layer is deposited on a surface of the solar cell (Al Montazer Mandong 2021).

ARCs are widely used today in the design of PV cells. Several studies have shown that single-layer coatings have a narrow reflectance band and present dissatisfaction in terms of their performance (Medhat et al. 2016; Dai et al. 2012). This type of technology, also called double-layer antireflection (DLARC) (Medhat et al. 2016; Dai et al. 2012; Chang et al. 2010; Richards Sep. 2003), is satisfactory in terms of performance only for broadband cells. Additional layers can also be increased to obtain minimal reflectance for a multitude of wavelengths (Asghar et al. 2004).

Many works have been reported on the ARCs with different materials such as SiN_X/SiN_X Sharma et al. (2017), SiO_2/TiO_2 Lien et al. (2006), Al_2O_3/TiO_2 Bahrami et al. (2013), and MgF_2/TiO_2 Medhat et al. (2016). However, an increase in J_{SC}, and η can be observed for anti-reflective coatings using silicon solar cells compared to a solar cell without coating when applying simulation software.

Some familiar research methods include transfer matrix method (TMM), Fresnel equations simplified by Rouard's method (Al Montazer Mandong 2021), etc. Unlike other methods, TMM method is much more efficient for the calculation of optical properties of a multilayer structure (Mbakop et al. 2020). Figure 1 shows the schematic diagram of a TPV composed a 1D-PhCs filter, and a DLARC or MLARC.

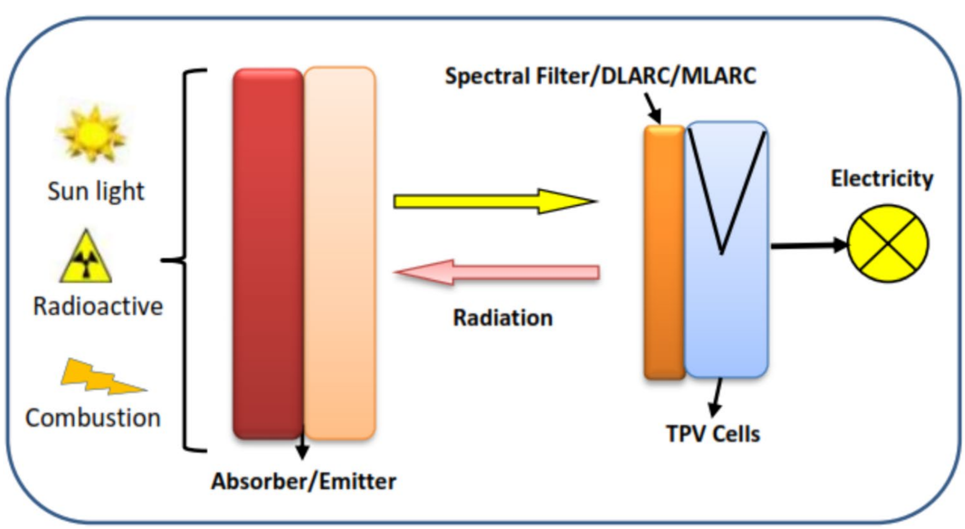

Fig. 1 Schematic illustration of a TPV device

In this article, a simulation study analyzes the optical properties, refractive index and thickness of DLARC and MLARC coatings applied to a TPV device. However, these coatings which have always been applied to PV devices will be compared to an optical filter. The method used and the theory of anti-reflective coating made it possible to determine the characteristics of each structure. Furthermore, GaSb TPV cell parameters such as short-circuit current (Isc), external quantum efficiency (EQE), and conversion efficiency are investigated for different angles of incidence.

Methods

Most photovoltaic cells are coated with anti-reflective (AR) coatings (ARC) to decrease the reflection of light on the cell. The characteristics of an ARC reduce multiple reflections and increase photocurrent in PV cells. A good design of this device makes it possible to reduce the reflectivity on the surface of the PV cell from 30% to less than 2% (Sharma 2018). However, to determine the reflectivity of ARCs, several methods are used such as: TMM, Fresnel's formula and Rouard's method (Medhat et al. 2016; Sahouane and Zerga 2014; Beye et al. 2013). Of all these methods, TMM is most widely used because it allows the components of the electric and magnetic fields of each multilayer structure to be associated (Beye et al. 2013).

The TMM method is generally used in the materialization of optical filters with photonic crystals. For a 1D system with refractive index n1 placed on a substrate with index ns, this method is expressed as follows (Tchoffo et al. 2022):

$$\begin{bmatrix} B \\ C \end{bmatrix} = \begin{bmatrix} cos\delta & \frac{isin\delta}{\eta} \\ \eta(isin\delta) & cos\delta \end{bmatrix} \begin{bmatrix} 1 \\ \eta_S \end{bmatrix} \quad (1)$$

where $\delta = \frac{2\pi n_1 d_1 cos\theta_1}{\lambda}$, is phase shift the film, d_1 is the film thickness, θ_1 is the diffraction angle related to the incidence angle θ_0 by Snell's law: $n_0 \sin\theta_0 = n_1 \sin\theta_1$ and η is the optical admittance with parallel and perpendicular components

$$\eta_{//} = \left(\sqrt{E_0/\mu_0 n}\right)/cos\theta \text{ and } \eta_{\perp} = \sqrt{E_0/\mu_0 \eta cos\theta}. \quad (2)$$

Single-layer anti-reflection coating (SLARC) is effective at a single wavelength, while double layer and multilayer anti-reflection coatings are effective over a wide range of wavelengths (Mbakop et al. 2016). It is this type of multilayer coating that is used for the design of photonic crystal (1D-PC) spectral filters. Thus, the above analysis (TMM) can be extended on DLARC as (Macleod and Macleod 2010):

$$\begin{bmatrix} B \\ C \end{bmatrix} = \begin{bmatrix} cos\delta_1 & \frac{isin\delta_1}{\eta_1} \\ \eta_1(isin\delta_1) & cos\delta_1 \end{bmatrix} \begin{bmatrix} cos\delta_2 & \frac{isin\delta_2}{\eta_2} \\ \eta_2(isin\delta_2) & cos\delta_2 \end{bmatrix} \begin{bmatrix} 1 \\ \eta_S \end{bmatrix} \quad (3)$$

This gives the reflection (r) and transmission (t) coefficients for a given assembly as (Beye et al. 2013; Macleod and Macleod 2010):

$$r = \frac{\eta_0 m_{11} + \eta_0 \eta_s m_{12} + m_{21} + \eta_s m_{22}}{\eta_0 m_{11} + \eta_0 \eta_s m_{12} + m_{21} + \eta_s m_{22}}, \quad (4)$$

$$t = \frac{2\eta_0}{\eta_0 m_{11} + \eta_0 \eta_s m_{12} + m_{21} + \eta_s m_{22}}. \quad (5)$$

where m_{11}, m_{12}, m_{21}, and m_{22} are the elements of the characteristic matrix obtained by multiplying the two matrices representing two layers, while η_0 and η_s are the admittance values of incident medium and the substrate. The energy coefficients (reflectance, transmittance are given by Sahouane and Zerga (2014):

$$R = |r|^2, \quad (6)$$

$$T = \frac{\eta_s}{\eta_0}|t|^2. \quad (7)$$

Theory

Theory of Antireflection-Coating DLARC and MLARC

In narrow wavelength ranges, minimum reflectance is obtained on solar cells from single-layer ARC (Martirosyan et al. 2007).

In the design of double and multilayer structures, the main parameters to take into consideration the refractive index n and the layer thickness d. However, the DLARC must satisfy the modeling of Eq. (8) when it is composed of a GaSb substrate having a top layer and a bottom layer. The reflectance becomes zero at certain wavelengths (Martirosyan et al. 2007; Lee et al. 1998):

$$n_2 = \sqrt{n_{GaSb}.n_1}. \quad (8)$$

Furthermore, the quarter-wave optical thickness is reached for each layer when the broadband reflectance centered on λ occurs (Lee et al. 1998):

$$n_1 d_1 = \frac{\lambda_{min}}{4} \text{and } n_2 d_2 = \frac{\lambda_{min}}{4}. \quad (9)$$

To obtain the best part of the energy distribution in the IR spectrum, the dual-layer AR configuration must be tuned to create minimum reflectance (Martirosyan et al. 2007).

In "Methods", we extensively developed the mathematical model of multilayer coatings. This section shows that by adjusting the refractive index and layer thickness, all reflected vectors should be minimized (Raut et al. 2011).

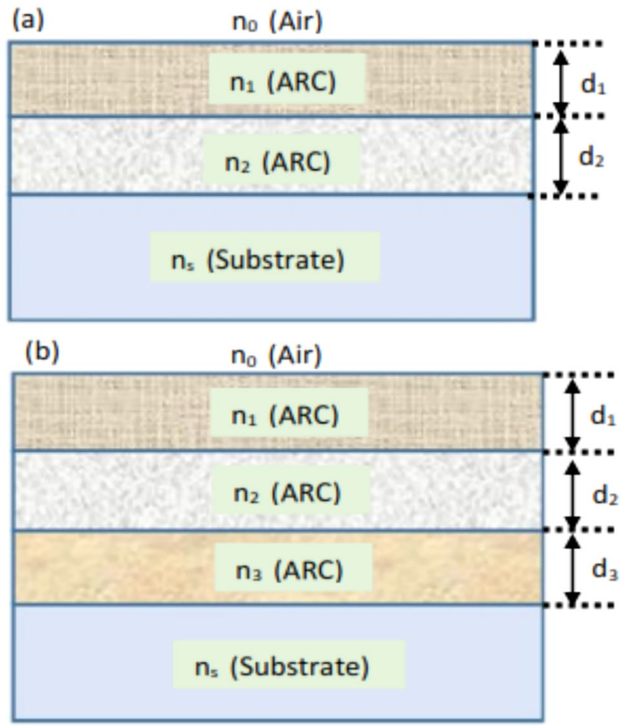

Fig. 2 Design diagram of antireflection coatings with **a** double layers (DLARCs) and **b** triple layers (MLARCs)

Figure 2 shows the schematic design for DLARC and MLARC.

Filter Design Theory

We present and analyze in this work a TPV conversion device having 1D-PhCs optical filters. these devices are composed of $(LH)^N$, with N periods, which transmit light to a GaSb cell. The different layers are designed and deposited on a quartz substrate. This system is compared to a filterless TPV system having an AR coating (DLARC and MLARC). However, the spectral domain chosen in this study is that of the IR domain.

The gap energy of GaSb materials is $E_g = 0.7$ eV and has a wavelength of $\lambda_g = 1.78$ µm (Mbakop et al. 2020). The distance between the transmitter and the cell is 1 cm. The different optical filters are deposited on a NaCl substrate. In a 1D-PhC optical filter the total photonic bandgap is non-existent. However, it is capable of giving full omnidirectional reflectance if combined with free space. For this, all angles of incidence must be superimposed. This principle can be used to improve TPV devices (Mbakop et al. 2020; Zaghdoudi et al. 2012; Fink et al. 1998; Liu et al. 2008).

One-dimensional SiO_2/TiO_2, SiO_2/ZnS, SiO_2/ZrO_2 and SiO_2/PbF_2 structures are essentially quarter-wave periodic multilayers films. However, Eq. (10) presents central wavelength at normal incidence (Mbakop et al. 2020):

$$\lambda_0 = \frac{1}{1 - \frac{2}{\pi} sin^{-1}\left(\frac{n_H - n_L}{n_H + n_L}\right)} \lambda_g, \tag{10}$$

At normal incidence, we have λ_g which represents the wavelength at normal incidence, while n_H and n_L designate the high and low refractive indices respectively. The following modeling is the representation of the thickness of the layer (Mbakop et al. 2020):

$$d_k = \frac{\lambda_0}{4 n_k}, \tag{11}$$

where n_k denotes its refractive index. In this paper, the wavelength was set in the near-infrared (NIR) range, normally between 800 and 1800 nm.

The central wavelengths are taken at $\lambda_g = 1200$ nm. Figure 3 is the representation of the model chosen in this work, 1D-PhC.

Material Choice

In mid-infrared spectral range, several semiconductors could be chosen as substrate materials, such as sapphire, CaF_2,

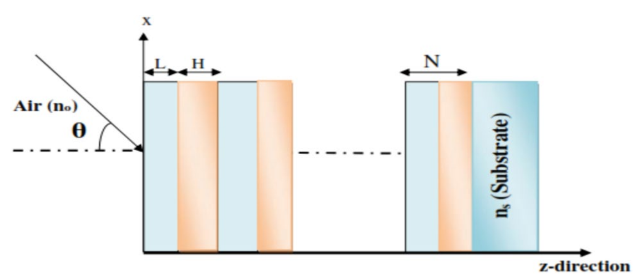

Fig. 3 TPV device composed of a 1D-PhC optical filter deposited on GaSb

Table 1 AR coating materials with their refractive indices (Sharma 2018)

Material	Refractive Index
MgF_2	1.38
Na_3AlF_3	1.35
CaF_2	1.43
SiO_2	1.46
Al_2O_3	1.73
PbF_2	1.76
ZrO_2	2.2
ZnS	2.36
TiO_2	2.4
Si	3.5

ZnSe, Si and Ge. In this paper, GaSb was chosen to be used as substrate material. Table 1 shows some frequently used AR cladding materials with their refractive indices.

The materials contained in this table will also be used in part of work concerning the design of 1D-PhC spectral filter.

Electrical Parameters

Conversion Efficiency

Making a cell with a high conversion efficiency requires improving the maximum power, P_m, and the short circuit current, I_{sc}. It can be obtained from the following equation (Medhat et al. 2016; Green 1982):

$$\eta = \frac{P_m}{P_{in}} = \frac{V_{oc} I_{sc} FF}{P_{in}}, \tag{12}$$

This formula is the representation of the different properties of the solar cell. V_{oc} is the open circuit voltage, P_{in} is the photon input power, and FF is the fill factor. The FF is very often used to determine the current–voltage (I-V) curve and its mathematical model is (Medhat et al. 2016; Vos 1983):

$$FF = \frac{V_m I_m}{V_{oc} I_{sc}}, \tag{13}$$

where I_m and V_m represents the current and voltage0 corresponding to the maximum power (P_m), respectively.

Results and Discussion

For this study, we present two models structural designs that can improve the efficiency of a TPV conversion system through its cell. Concerning the first method, it is a question of designing a DLARC and a MLARC on a GaSb substrate and seeing which one displays better optical properties. To achieve the expected results, several structures have been examined, namely: SiO_2/MgF_2, SiO_2/Al_2O_3, SiO_2/ZrO_2, SiO_2/ZnS and SiO_2/TiO_2 for the DLARC and $MgF_2/SiO_2/TiO_2$, $Na_3AlF_3/SiO_2/TiO_2$ and $CaF_2/SiO_2/TiO_2$ for MLARC, in order to determine the device that best fits our work. In second model, we have designed a bandgap 1D-PhC filter. Each 1D-PhC includes layers with different refractive indices. The band gap of this device is directly controlled by the parameters of the layers such as the thickness d and the refractive index (Mbakop et al. 2020). The number of periods is fixed at 10, i.e. there are a total of 20 layers made up of 10 layers for materials with high refractive indices (H) and 10 layers for materials with low refractive indices (L). As for the DLARC and MLARC structures, a study is made on several 1D-PhC filters, SiO_2/TiO_2, SiO_2/ZnS, SiO_2/ZrO_2 and SiO_2/PbF_2, to come out with the best one. In this work, we present the performance of the TPV cell in both models. However, these performances depend exclusively on the angle of incidence. The different results presented in this study are solely based on the polarization mode of the electromagnetic field which is composed of the electric transverse mode TE and magnetic transverse mode TM. These results will be presented in the NIR wavelength range. Appealing to the TMM method, we have designed a DLARC, MLARC and a 1D-PhC filter in the spectral range 1200−1800 nm. The central wavelength is equal to 1200 nm.

Study of the Reflectance and Transmittance of Different Structures of the Filter

The results presented in Fig. 4 evaluate optical properties such as reflection and transmission in TM polarization mode. The filter is designed in the mid-IR spectral range and the period is fixed at $P = 10$.

In this part, we evaluate the reflectance and transmittance of different filter structures in near-IR range. The simulation results of Fig. 4 allow us to select structure which exhibits the best spectral response, in order to optimize the electrical parameters of the TPV cell.

The number of periods is the central wavelength corresponding to $P = 10$ and $\lambda o = 1200$ nm. As can be observed from Fig. 4a and b, the ZnS/SiO_2 structure displays the smallest bandwidth and achieves 100% reflectance and transmittance. Its opening and closing wavelengths are between $\lambda_1 = 1039$ nm and $\lambda_2 = 1440$ nm, for a bandwidth $\Delta\lambda = 399$ nm for reflectance and $\Delta\lambda = 280$ nm for transmittance. The second structure (TiO_2/SiO_2) *exhibits* a wider bandwidth than the previous one and also reaches a maximum of 100% reflectance and transmittance. Its wavelengths are between $\lambda_1 = 1020$ and $\lambda_2 = 1463$ nm for a bandwidth of $\Delta\lambda = 443$ nm for reflectance and $\Delta\lambda = 340$ nm for transmittance. The third structure (Bi_2O_3/SiO_2) also shows a maximum of 100% reflectance and transmittance, but with greater bandwidth. This structure has opening wavelength $\lambda_1 = 1010$ and closing one $\lambda_2 = 1472$ nm for a bandwidth of $\Delta\lambda = 462$ nm for the reflectance and of $\Delta\lambda = 400$ nm for the transmittance. The last structure presented in this study of the various filters is Si/SiO_2, which has already been the subject of several researches (Babiker et al. 2014). It is observed from Fig. 4 that this structure performs better than previous structures and has a large bandwidth. Its opening wavelength is $\lambda_1 = 940$ and that of closing one is $\lambda_2 = 1655$ nm for a bandwidth of filter. It also displays a greater bandwidth, $\Delta\lambda = 715$ nm, for reflectance and $\Delta\lambda = 700$ nm for transmittance. We observe a similarity with the work obtained by Li et al. (Li et al. 2015a, b) and Mbakop et al. (2016). The TPV cell has good efficiency when the optical filter satisfies a homogeneous linear device. Table 2 shows the transmission

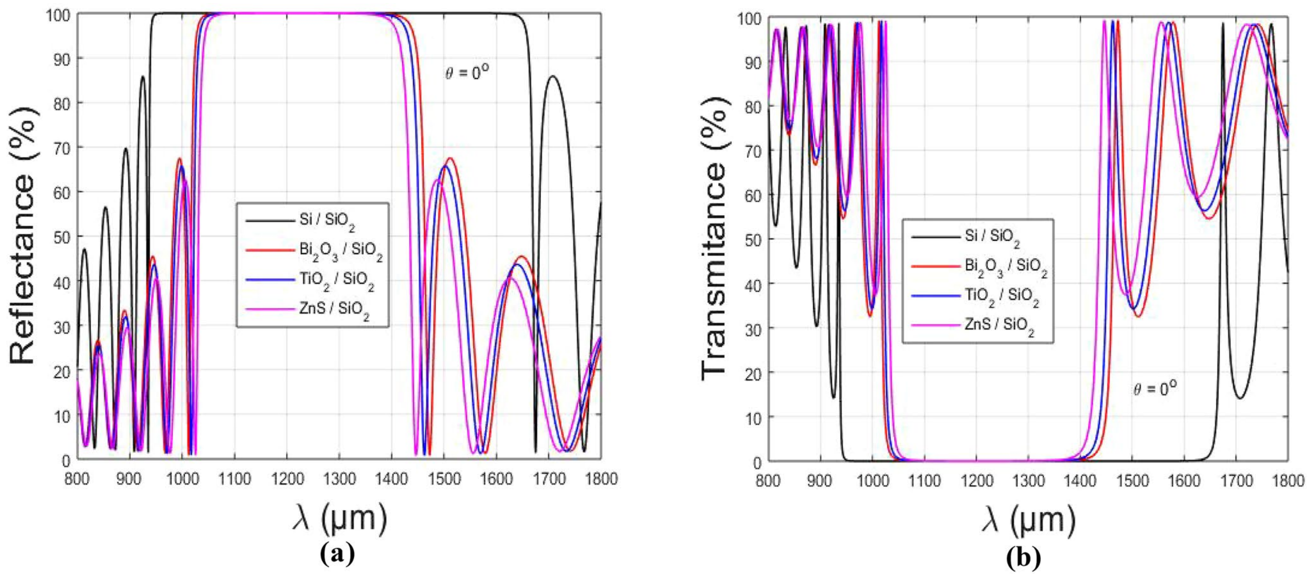

Fig. 4 Evaluation of reflectance (**a**) and transmittance (**b**) of different filter structures

Table 2 Transmittance and reflectance values for the different structure

	R			*T*		
Structures	λ_1 (nm)	λ_2 (nm)	$\Delta\lambda$ (nm)	λ_1 (nm)	λ_2 (nm)	$\Delta\lambda$ (nm)
Si/SiO_2	940	1655	715	950	1650	700
Bi_2O_3/SiO_2	1010	1472	462	1050	1450	400
TiO_2/SiO_2	1020	1463	443	1060	1400	340
ZnS	1040	1439	399	1070	1350	280

and reflectance values for different devices at a period of $P = 10$.

Effect of Incident Wave on Transmission for TE and TM Modes

Figure 5 shows the transmittance of the filter across the TPV cell when varying the angle. The structure chosen for the study of angle variations was SiO_2/TiO_2. The wave coupling mode is TM and TE for a period of $P = 10$.

We observe in Fig. 5 a variation of the angle for an unchanged period P = 10. the structure chosen in this section is SiO_2/TiO_2. The number of periods remains unchanged, $N = 10$. The transmission spectra of the proposed structure in both TE and TM modes are shown in this figure. The different incidence angles taken into account in this study vary from 0º to 45º and were chosen equal to 0º, 20º, 30º and 45º. The central wavelength is observed in Fig. 5 to 1200 nm.

Thus, we see that the transmission band space of the TE and TM modes remains unchanged when the wave is polarized at normal incidence. However, a change in polarization occurs between the two modes (TE, TM) when the incidence varies up to 20°. The same phenomenon is observed when the angle is increased from 30º to 45º. In the bandwidth region, a decrease in transmission is observed with increasing incidence. The stopband shifts towards shorter wavelengths with increasing angle of incidence (Babiker et al. 2014). In Fig. 5a, the TM polarization mode decreases rapidly with increasing incident angle (Pirvaram et al. 2021). The local field of a one-dimensional photonic crystal can be enhanced when the angle is taken at an oblique incidence. This can be much better than that of a normal incidence (Mbakop et al. 2016). Table 3 presents the different transmittance values with variation in incidence.

Reflectance and Transmittance of DLARC and MLARC

Figure 6 presents the behavior of the optical properties of different DLARC and MLARC structures for a TPV cell.

As mentioned above, according to the literature, SLARC structure does not cover the wide spectrum range and can only minimize reflection at one wavelength. However, the DLARC or MLARC systems can be designed for the TPV cell. The latter will be present in the following section.

Several structures were tested in order to choose the one exhibiting the best results. The reflectance (Fig. 6a, c) and

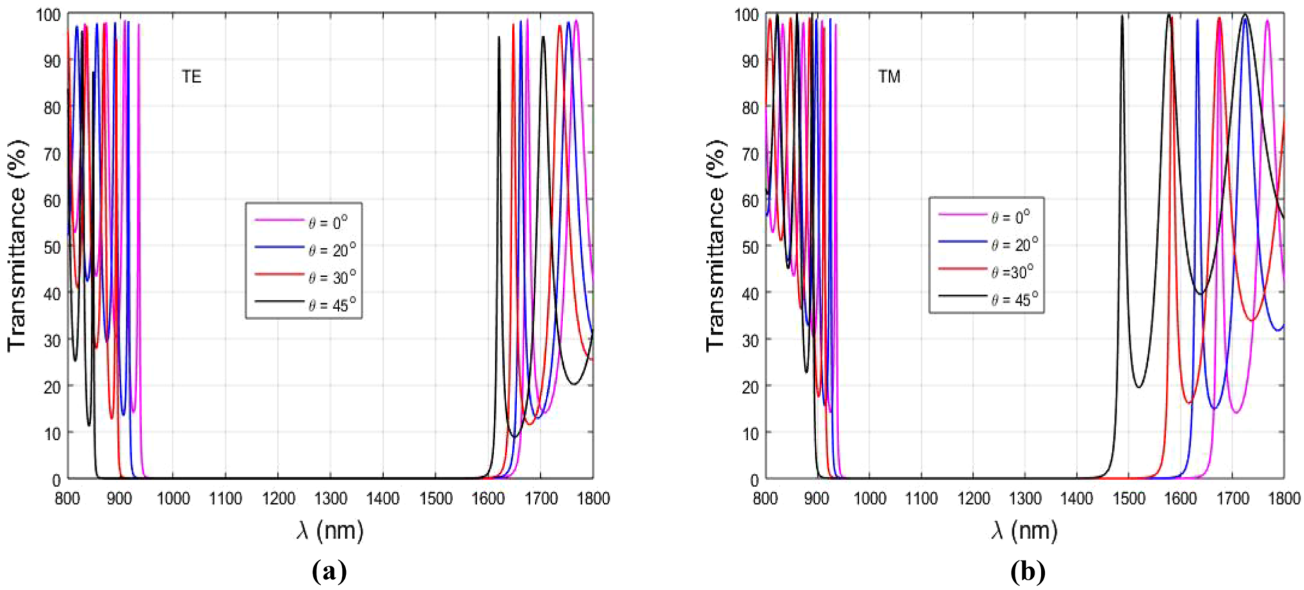

Fig. 5 Effect of angle variation on transmission for SiO_2/TiO_2 structure

Table 3 Transmission values after variation of incidence for TE and TM modes

Structure	Angles (°)	Modes					
		TE			TM		
		λ_1	λ_2	$\Delta\lambda$	λ_1	λ_2	$\Delta\lambda$
Si/SiO_2	0^0	850 nm	1600 nm	750 nm	900 nm	1450 nm	550 nm
	20^0	900 nm	1620 nm	720 nm	930 nm	1550 nm	620 nm
	30^0	930 nm	1630 nm	700 nm	940 nm	1600 nm	660 nm
	45^0	950 nm	1640 nm	690 nm	950 nm	1650 nm	700 nm

transmittance (Fig. 6b, d) spectra were plotted using the TMM method. Figure 6a and b present the results obtained for DLARC. For the SiO_2/MgF_2 structure, the reflectance has a value of 9–37%, and transmittance is of 90% in the wavelength ranging from 800 to 1800 nm. For SiO_2/Al_2O_2 structure, the reflectance decreases until a value of 6−20% for a transmittance of 96%. In the same wavelength range, the SiO_2/ZrO_2 structure displays a reflectance of 7%, with a relative increase in transmittance up to 98%. The reflectance decreases to 4%, while the transmittance is continuously increasing and reaches a value of 99.5% for the SiO_2/ZnS structure. The last structure, SiO_2/TiO_2, shows better results with respect to the previous ones. This structure reaches values of 2% and 100% representing the reflectance and transmittance values respectively. These values are taken over a wavelength range of 800 to 1800 nm, which is linked to the work of Lien et al. (2006). Furthermore, for DLARC configuration, the reflectance curve is W-shaped, i.e. the reflectance becomes minimum at two wavelengths. In general, in this type of antireflection coating, the choice of materials with refractive indices lower than 1.5, such as SiO_2, CaF_2 or MgF_2, can be appropriate for the first layer.

Therefore, the $CaF_2/SiO_2/TiO_2$ structure has a reflectance of 0.7% and a transmittance of 99.8% on its first peak located in the wavelength range of 1000 to 1100 nm. Furthermore, these properties (reflectance, transmittance) are canceled on the second peak, between 1300 and 1400 nm. Our results indicated that unlike the others, the Na3AlF3/SiO2/TiO2 structure is the one that presents better efficiency. This is achieved by its very small reflectance and lower transmittance in the wavelength range of 1050 to 1400 nm, in the NIR domain. The results presented in this work are contrasting to those of Al Montazer Mandong (2021), which presents the $MgF_2/SiO_2/TiO_2$ structure to be the best in the visible spectrum. Table 4 summarizes the average reflectance and transmittance of each structure for DLARC and MLARC.

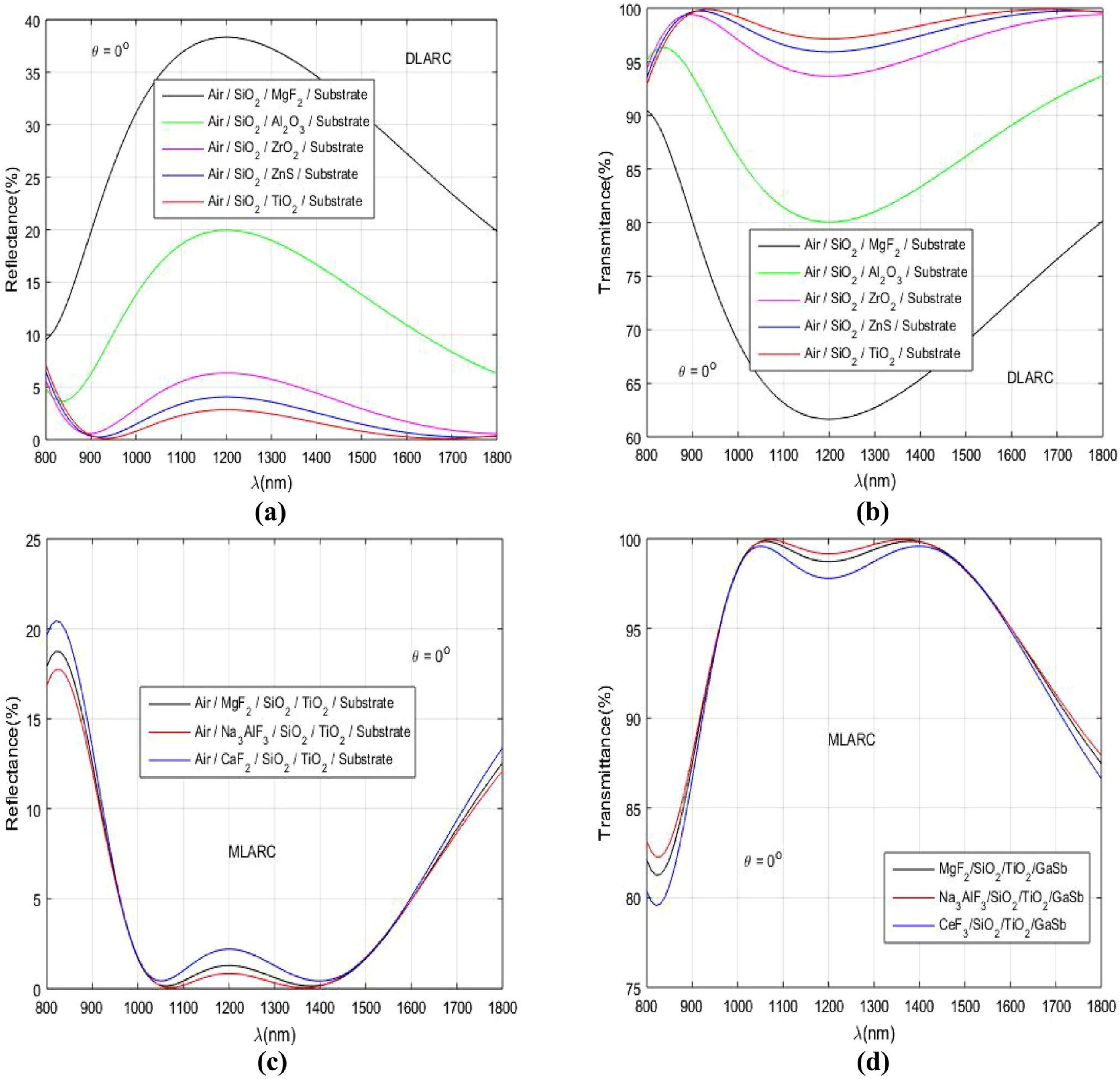

Fig. 6 Reflectance spectra of **a** DLARC and **c** MLARC structures. Transmittance spectra of **b** DLARC and **d** MLARC structures on GaSb substrate

Oblique Incidence of Antireflection Coatings of DLARC and MLARC

Figure 7 shows the influence of oblique incidence on the reflection of different DLARC and MLARC structures from the TPV cell. The structures chosen for this purpose are SiO_2/TiO_2 for the DLARC configuration and the $Na_3AlF_3/SiO_2/TiO_2$ for the MLARC one. The study was made for the two polarization modes, TM and TE.

Figure 7 shows spectral dependence of reflectance for different angles of incidence and their influence on performance of GaSb cell of a TPV system. The behavior of different configurations, DLARC and MLARC, in both TE and TM polarization modes is presented in Fig. 7, respectively. The TMM method allowed calculations to be made numerically on angles such as 0º, 20º, 30º and 40º. As can be seen in Fig. 7a and b, the reflectance curve in the two polarization modes for the DLARC is W-shaped. This means that for two specific wavelengths, the reflectance is at its lowest level. Moreover, one can observe that for both polarization modes, reflectivity increases together with the incidence. For the TE polarization in

Table 4 Reflectance and transmittance values of each structure for DLARC and MALRC

	Structures	Reflectance (%)	Trans-mittance (%)
DLARC	SiO_2/MgF_2	9.0–37.0	90.0
	SiO_2/Al_2O_3	6.0–20.0	96.0
	SiO_2/ZrO_2	7.0	98.0
	SiO_2/ZnS	4.0	99.5
	SiO_2/TiO_2	2.0	100
MLARC	$CaF_2/SiO_2/TiO_2$	1.5	99.0
	$MgF_2/SiO_2/TiO_2$	0.8	100
	$Na_3AlF_3/SiO_2/TiO_2$	0.3	100

Fig. 7a, we observe a shift in the reflectance towards small wavelength values as the incidence increases from 0° to 40°. However, when the incidences vary from 0° to 30°, the reflectance curve remains stable over the entire wavelength range.

Instead, for TM polarization (Fig. 7b), the reflectance curves do not change despite variations in the angle of incidence. Furthermore, Fig. 7b showing the TM polarization, the reflectance remains stable even if the angle of incidence is varied. However, in Fig. 7a and in the same way as in the case of TM polarization, for TE polarization the reflectance curve also remains stable regardless of variations in the angle of incidence. However, a significant increase in reflectance is observed when the angle of incidence reaches 40º. This behavior is in agreement with the works of Diaye et al. (Beye et al. 2013) and Sharma (2019).

Figure 7c and d show the reflectance spectra for the MLARC structure at different angles of incidence and for the two polarization modes. As can be seen in this figure, the response of the reflectance curve is quite acceptable up to around 20º−30°. Furthermore, the reflectance curves are blue-shifted for the TE polarization as can be observed in Fig. 7c is relatively stable in TM polarization as observed in Fig. 7d.

We In this study it is observed that, for both types of AR structures, the design is made to operate at normal incidence and can then be used over a limited range of oblique incidence angles up to about 30º. If a particular angle of incidence is preferred, it is possible to design the antireflection coating to match that angle. However, like the case of normal design, the effectiveness of this method will be over an angular width of approximately 30° about the preferred angle. Our results reveal that the MLARC configuration shows better reflectance results for different values of the incidence angle, compared to DLARC.

Antireflection Coatings at a Chosen Oblique Incidence

Figure 8 shows influence oblique incidence on reflectance of a DLARC for the GaSb TPV cell, at a chosen angle of oblique incidence θa. The study is made for the two polarization modes, TM and TE.

As mentioned above, the design can be matched at a particle angle of incidence. In this study, we chose $\theta_a = 30º$ and redesigned the two-layer structure. From Fig. 8a (TE polarization mode) it can be seen that the angle of incidence $\theta = 0º$ is only appropriate for a chosen angle of incidence $\theta_a = 30º$. Figure 8b presents the corresponding reflectance in TM mode, which cannot be matched simultaneously with that in the TE polarization mode. It can be observed that the curves get closer towards longer wavelengths for increasing angles of incidence from 0º to 40º. Furthermore, the chosen angle $\theta_a = 30º$ is well suited to this polarization mode.

In GaSb TPV conversion cells, using AR coatings, it is possible to choose an oblique incidence to obtain optimum efficiency. The limiting incidence angle in this work is fixed at $\theta_a = 30º$ and corresponds to the TM polarization mode.

Electrical Parameters of GaSb Cell

Figure 9 presents *I-V* current–voltage characteristic curves of the GaSb cell from the TPV system, studied for different structures proposed in this work.

To obtain better system performance after improving the reflectance and transmission, the improvement of electrical properties (I-V) of all AR devices can be seen in Fig. 9. The results of the I-V electrical properties of the GaSb cell without ARC, with DLARC (SiO_2/TiO_2), MLARC ($Na_3AlF_3/SiO_2/TiO_2$) and for optical filters are shown in Fig. 9.

The incident radiation from the TPV transmitter is in the IR range varying from, 800 to 1800 nm.

That is why TPV cells need to use smaller semiconductors such as GaSb, which has an energy of 0.7 eV and wavelength of 1.7 µm. Knowing that incident power on a solar cell is around 0.1 W/cm^2, that on TPV cell typically of 10 W/cm^2. It is much more higher than solar energy incident on surface of earth, which gives the main attraction of TPV cells (Coutts 2001, 1999).

The cell performances are evaluated for different structures studied (DLARC, MLARC and Optical Filter) under blackbody radiation (blackbody radiator). In the case of filter (red dotted courve), only a small fraction of photons created by radiative recombination can escape from cell due to total reflection, since GaSb has a large refractive index of 3.8 (Zenker et al. 2001; Coutts 1999; Balasubbareddy 2023; Balasubbareddy and Divyanshi 2022; Balasubbareddy et al. 2023). Figure 9 emphasizes a significant increase in the short circuit current for different structures used, compared to that

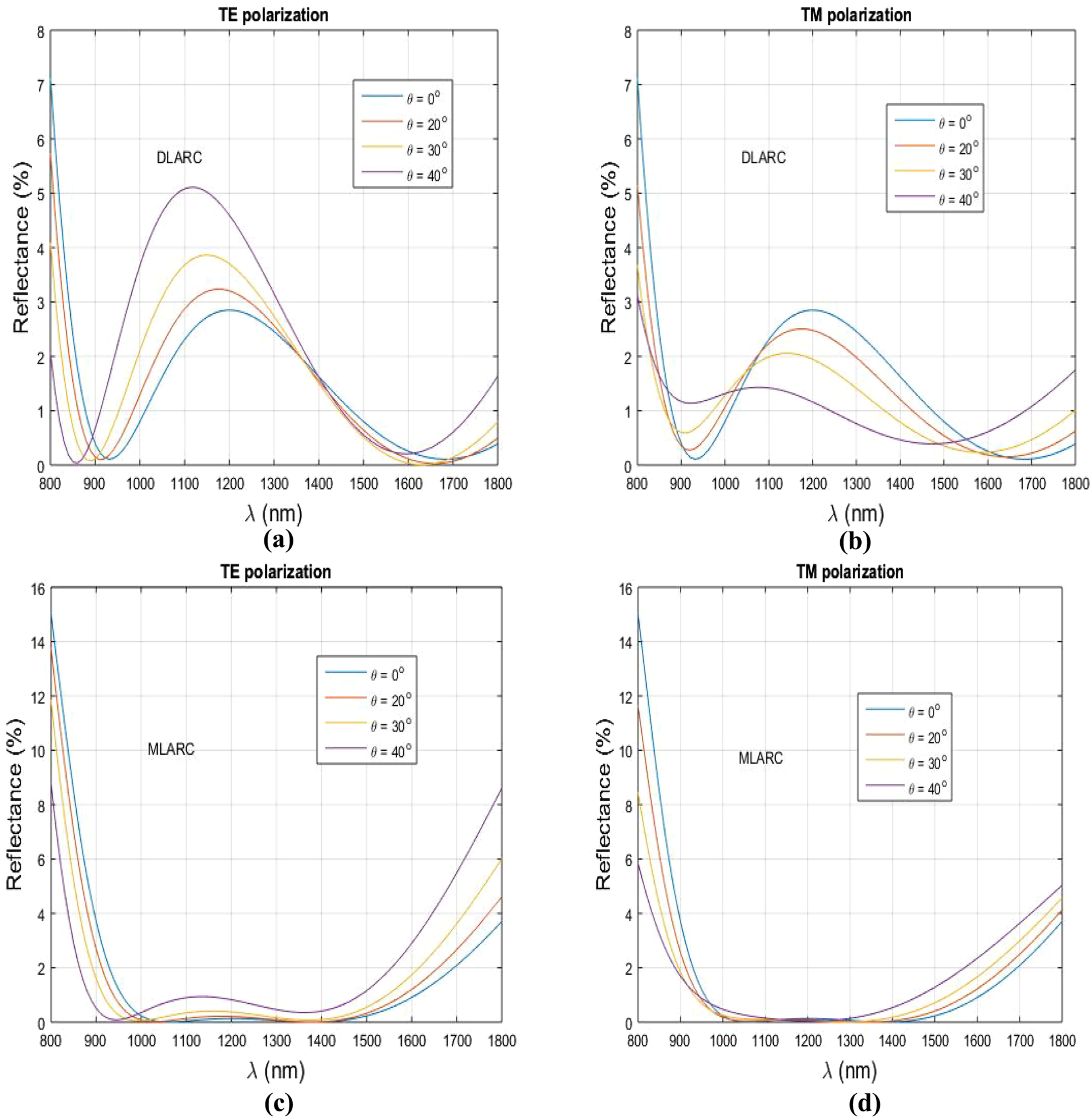

Fig. 7 Oblique incidence reflectance spectra for a DLARC structure and for MLARC structure

of the cell without AR coating. However, the open-circuit voltage and the fill factor do not change. Instead, *I-V* characteristics of Optical Filter show the best results. The efficiency of GaSb cell with Optical Filter is 24.56%, while that of DLARC and MLARC ($Na_3AlF_3/SiO_2/TiO_2$) cells exhibits an increase from 21.98 to 22.77%, compared to the cell without AR coating, for which the efficiency is of 15.76%.

It is worth to mention that the value of the power density extracted from TPV cell is much greater than one as expects from a silicon PV cell. Table 5 illustrates the I-V performance of different solar cells ARC, as well as with Optical Filter.

Conclusion

In this work, the TMM was extensively developed to evaluate the efficiency and power density of DLARC and MLARC solar cells. In order to improve the performance

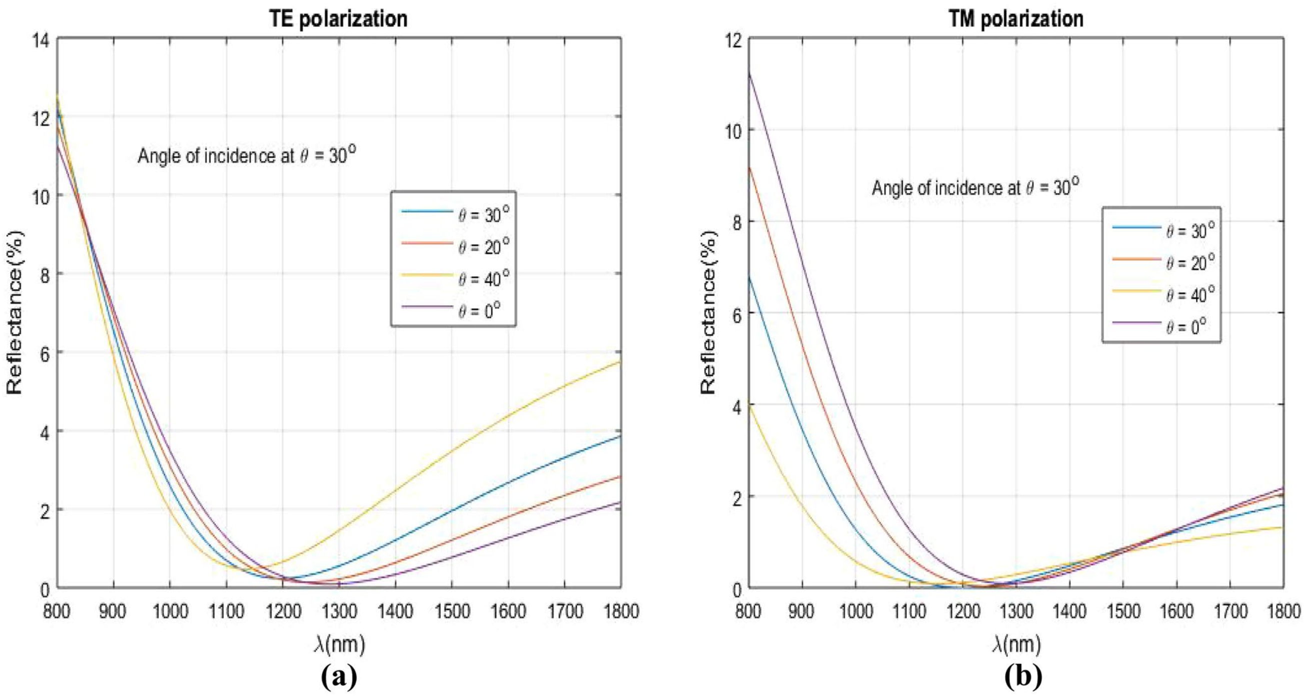

Fig. 8 Oblique incidence at $\theta_a = 30º$ for the two polarization modes

Fig. 9 Presents the behavior of the electrical parameters of the GaSb cell

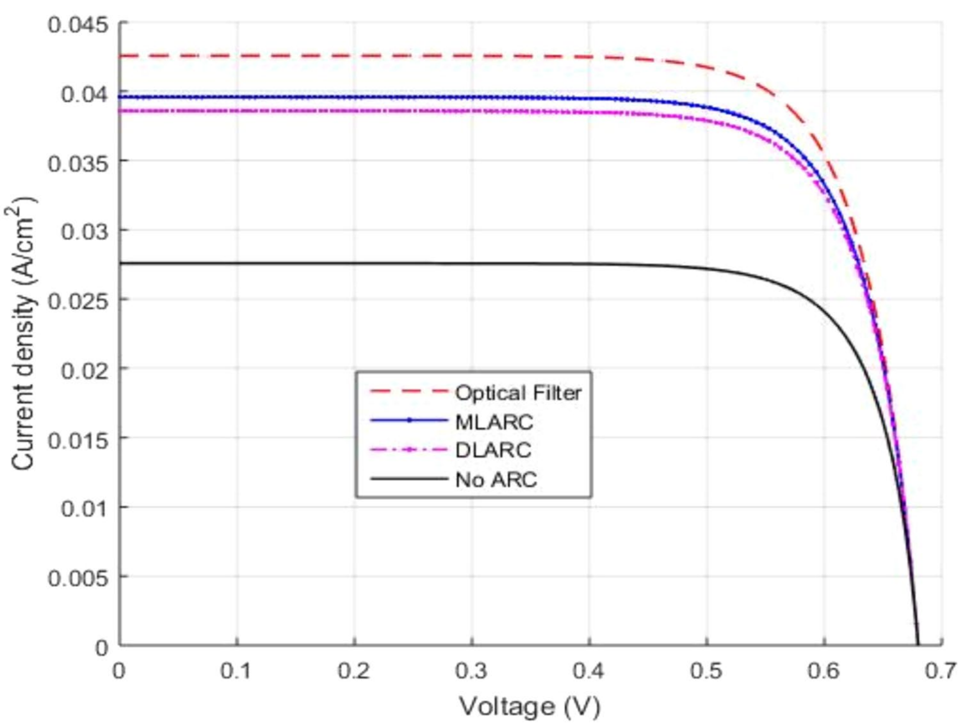

Table 5 Electrical performance of different types of GaSb cells

ARC and filter design	I_{sc} (mA/cm^2)	V_{oc} (V)	FF (%)	η(%)
No ARC	27.6	0.6798	84.0	15.76
DLARC (SiO_2/TiO_2)	38.6	0.6799	84.3	21.98
MLARC ($Na_3AlF_3/SiO_2/TiO_2$)	39.6	0.6799	84.5	22.77
Optical Filter (TiO_2/SiO_2)	42.6	0.6799	84.8	24.56

of the GaSb cell used in TPV, the results were compared to those obtained with a 1D-PhC filter. Among of the proposed structures. Si/SiO_2 was chosen for the filter, SiO_2/TiO_2 for the DLARC and $Na_3AlF_3/SiO_2/TiO_2$ for the MLARC configurations. All structures were designed for the NIR region, in the spectral range of 800−1800 nm, under an emitter temperature of 1500 K. This numerical method also allows to analyze influence of reflectance, transmittance and incidence on behavior of different structures. The results reveal that, the reflectance and the transmittance at the front surface of GaSb cell with DLARC (SiO_2/TiO_2) are of 2% and 100%, respectively while 0.3% and 100%, have been obtained for the MLARC ($Na_3AlF_3/SiO_2/TiO_2$) respectively. Using an optical filter leads to values of 100% for reflectance and transmittance, which is valuable as it covers the peak region of the near infrared spectrum.

The influence of angle of incidence on performance of GaSb TPV cell with the three structures was studied comparatively, for two polarization modes, TE and TM. For DLARC and MLARC configurations, the obtained results show that the incidence angle of strongly affects the antireflection properties beyond 30º. Thus, the incidence angle was fixed at 30°, value for which a better result is provided by TM polarization. In addition, it has been observed that, the optical filter has no sensitivity at all angles of incidence. Furthermore, TM polarization is more sensitive to variation the angle on incidence than TE polarization, and stopband decreases and shifts to shorter wavelengths as the incidence increases. Short circuit current density and efficiency of all GaSb cells: without ARC, with DLARC, MLARC and filter was also examined. The obtained values were found to be of 27.6 mA/cm^2 and 15.76%, 38.6 mA/cm^2 and 21.98%, 39.6 mA/cm^2 and 22.77%, and 42.6 mA/cm^2 (a significant increase) and 24.56%, respectively. The considerable reduction in optical properties and the increase in electrical properties of cell greatly improve the light trapping performance of TPV cells, due to plasmonic forward light scattering effect. In the present study, it has been demonstrated that, although the antireflection configurations (DLARC and MLARC) are effective for the PV cell itself, they are not suitable for application in TPV conversion systems. In GaSb thermophotovoltaic systems, only optical filters are able to provide spectral and directional coherence with the GaSb cell. Therefore, by selecting the best combination of materials, performances of TPV or PV devices can be improved appealing to accurate simulations.

Acknowledgements The authors acknowledge the Alliance Universitaire de la Francophonie (AUF) for the funding as the staff of the Faculty of Physics of the University "Alexandru Ioan Cuza" of Iasi

Author contributions The authors carried out this study independently and comprehensively as part of their academic research work.

Funding This study was not funded by the various academic institutions involved.

Data availability The datasets used and/or analyzed during the current study are available from the corresponding author on reasonable request.

Declarations

Conflict of Interest Authors declare no conflict of interest.

References

Al Montazer Mandong AU (2021) Fresnel calculations of double/multilayer antireflection coatings on silicon substrates

Asghar MH, Khan MB, Naseem S (2004) Designing bandpass filters in 8–14 µm range for Si and Ge substrates. Semicond Phys Quantum Electron Optoelectron 7(4):355–359

Babiker SG, Shuai Y, Sid-Ahmed MO and Xie M (2014) One-dimensional Si/SiO_2 photonic crystals filter for thermophotovoltaic applications. In: WSEAS Trans. Appl. Theor. Mechan., p 9

Bahrami A, Mohammadnejad S, Abkenar NJ, Soleimaninezhad S (2013) Optimized single and double layer antireflection coatings for GaAs solar cells. Int J Renew Energy Res 3(1):79–83

Balasubbareddy M (2023) MATLAB software/code for optimal placement of GIPFC device in power networks using AALO algorithm. Software Impacts 17:100550

Balasubbareddy M, Divyanshi D (2022) ' Salp swarm algorithm for solving optimal power flow problem with thyristor-controlled series capacitor. J Electron Sci Technol 20:100156

Balasubbareddy M, Dwivedi D, Murthy GVK, Kumar KS (2023) Optimal power flow solution with current injection model of generalized interline power flow controller using ameliorated ant lion optimization. Int J Electr Comput Eng 13(1):1060–1077

Belhadj W, Timoumi A, Dakhlaoui H, Alhashmi Alamer F (2022) Design and optimization of one-dimensional TiO_2/GO photonic crystal structures for enhanced thermophotovoltaics. Coatings 12(2):129. https://doi.org/10.3390/coatings12020129

Beye M, Faye ME, Ndiaye A, Ndiaye F, Maiga AS (2013) Optimization of SiNx single and double layer ARC for silicon thin film solar cells on glass. Res J Appl Sci Eng Technol 6(3):412–416

Chang C-H, Waller L, Barbastathis G (2010) Design and optimization of broadband wide-angle antireflection structures for binary diffractive optics. Opt Lett 35(7):907–909

Coutts TJ (1999) A review of progress in thermophotovoltaic generation of electricityfnafnaI began writing this paper immediately after the Third nrel Conference on Thermophotovoltaic Genertion of materials, devices, and systems; substantial gains in fundamental understanding and performance of the quaternary alloy GaInAsSb; the introduction of new radiator concepts; and more attention being paid to modeling of both real and conceptual systems. There was also further evidence of interest in non-military applications, particularly from the European and Japanese attendees. Renew Sustain Energy Rev 3(2–3):77–184. https://doi.org/10.1016/S1364-0321(98)00021-5

Coutts TJ (2001) An overview of thermophotovoltaic generation of electricity. Sol Energy Mater Sol Cells 66(1–4):443–452

Dai W, Yap D, Chen G (2012) Wideband enhancement of infrared absorption in a direct band-gap semiconductor by using nonabsorptive pyramids. Opt Express 20(104):A519–A529

De Vos A (1983) The fill factor of a solar cell from a mathematical point of view. Sol Cells 8(3):283–296

Donne AL, Scaccabarozzi A, Tombolato S, Binetti S, Acciarri M, Abbotto A (2013) Solar photovoltaics: a review. Rev Adv Sci Eng 2(3):170–178. https://doi.org/10.1166/rase.2013.1030

Fink Y et al (1998) A dielectric omnidirectional reflector. Science 282(5394):1679–1682

Green MA (1982) Solar cells: operating principles, technology, and system applications. Englewood Cliffs

Gupta MVNS, Ameen E, Unnikrishnakurup S, Balasubramaniam K, Veeraragavan A, Pesala B (2021) Spectral filtering of sub-bandgap radiation using all-dielectric gratings for thermophotovoltaic applications. J Photonics Energy. https://doi.org/10.1117/1.JPE.11.015501

Lee J, Tanaka T, Sasaki S, Uchiyama S, Tsuchiya M, Kamiya T (1998) Novel design procedure of broad-band multilayer antireflection coatings for optical and optoelectronic devices. J Light Technol 16(5):884–891

Li H, Haus JW, Banerjee PP (2015a) Application of transfer matrix method to second-harmonic generation in nonlinear photonic bandgap structures: oblique incidence. JOSA B 32(7):1456–1462

Li H, Haus JW, Banerjee PP (2015b) Second harmonic generation at oblique angles in photonic bandgap structures. Nonlinear Frequency Gener Convers 9347:186–192

Lien S-Y, Wuu D-S, Yeh W-C, Liu J-C (2006) Tri-layer antireflection coatings (SiO_2/SiO_2–TiO_2/TiO_2) for silicon solar cells using a sol–gel technique. Sol Energy Mater Sol Cells 90(16):2710–2719

Liu G, Xuan Y, Han Y, Li Q (2008) Investigation of one-dimensional Si/SiO_2 hotonic crystals for thermophotovoltaic filter. Sci China Ser E Technol Sci 51(11):2031–2039

Macleod HA, Macleod HA (2010) Thin-film optical filters. CRC Press

Martirosyan KS, Hovhannisyan AS, Aroutiounian VM (2007) Calculation of reflectance of porous silicon double-layer antireflection coating for silicon solar cells. Phys Status Solidi C 4(6):2103–2106

Mbakop FK, Djongyang N, Raïdandi D (2016) One–dimensional TiO_2/SiO_2 photonic crystal filter for thermophotovoltaic applications. J Eur Opt Soc-Rapid Publ 12(1):1–9

Mbakop FK, Djongyang N, Ejuh GW, Raïdandi D, Woafo P (2017) Transmission of light through an optical filter of a one-dimensional photonic crystal: application to the solar thermophotovoltaic system. Phys B Condens Matter 516:92–99

Mbakop FK, Tom A, Dadjé A, Vidal AKC, Djongyang N (2020) One-dimensional comparison of TiO_2/SiO_2 and Si/SiO_2 photonic crystals filters for thermophotovoltaic applications in visible and infrared. Chin J Phys 67:124–134

Mbakop FK, Tom A, Dadjé A, Vidal AKC, Djongyang N (2020) One-dimensional comparison of TiO_2/SiO_2 and Si/SiO_2 photonic crystals filters for thermophotovoltaic applications in visible and infrared. Chin J Phys 67:124–134. https://doi.org/10.1016/j.cjph.2020.06.004

Medhat M, El-Zaiat E-S, Farag S, Youssef G, Alkhadry R (2016) Enhancing silicon solar cell efficiency with double layer antireflection coating. Turk J Phys 40(1):30–39

Pirvaram A, Talebzadeh N, Rostami M, Leung SN, O'Brien PG (2021) Evaluation of a ZrO_2/ZrO_2-aerogel one-dimensional photonic crystal as an optical filter for thermophotovoltaic applications. Therm Sci Eng Prog 25:100968. https://doi.org/10.1016/j.tsep.2021.100968

Raut HK, Ganesh VA, Nair AS, Ramakrishna S (2011) Anti-reflective coatings: a critical, in-depth review. Energy Environ Sci 4(10):3779–3804

Richards BS (2003) Single-material TiO_2 double-layer antireflection coatings. Sol Energy Mater Sol Cells 79(3):369–390. https://doi.org/10.1016/S0927-0248(02)00473-7

Sahouane N, Zerga A (2014) Optimization of antireflection multilayer for industrial crystalline silicon solar cells. Energy Procedia 44:118–125

Sathya P and Swarna Priya RM (2019) Numerical modeling and simulation of thermophotovoltaic cell using COMSOL. In: 2019 Innovations in Power and Advanced Computing Technologies (i-PACT), vol. 1, pp 1–5

Sharma R (2018) Silicon nitride as antireflection coating to enhance the conversion efficiency of silicon solar cells. Turk J Phys 42(4):350–355

Sharma R (2019) Effect of obliquity of incident light on the performance of silicon solar cells. Heliyon 5(7):e01965

Sharma R, Amit G and Ajit V (2017) Effect of single and double layer antireflection coating to enhance photovoltaic efficiency of silicon solar. J Nano Electron Phys 9(2):02001

Tchoffo FH, Mbakop FK, Nsouandele JLDB, Djongyang N (2022) Light transmission through one-dimensional photonic crystal filters for thermophotovoltaic applications. J Photonic Mater Technol 7(2):16–25

'Wolf (1976) Performance analyses of combined heating and photo.pdf

Zaghdoudi J, Maaloul N, Kanzari M (2012) Studies of optical properties of symmetrical quasi-periodic photonic crystals. Opt Photon J 2(4):270–277

Zenker M, Heinzel A, Stollwerck G, Ferber J, Luther J (2001) Efficiency and power density potential of combustion-driven thermophotovoltaic systems using GaSb photovoltaic cells. IEEE Trans Electron Devices 48(2):367–376

Zhang C, Tang L, Liu Y, Liu Z, Liu W, Qiu K (2020) A novel thermophotovoltaic optical cavity for improved irradiance uniformity and system performance. Energy 195:116962. https://doi.org/10.1016/j.energy.2020.116962